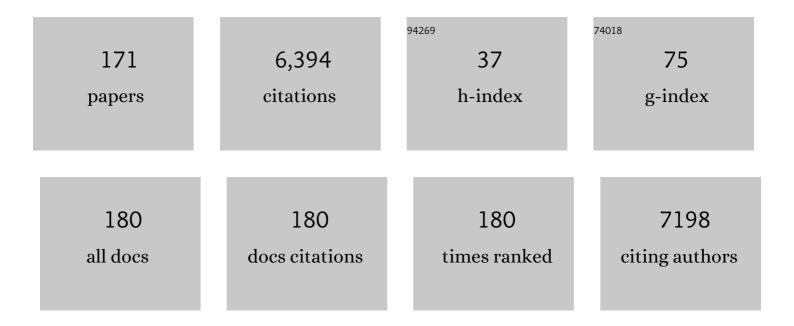
Jon P Wright

List of Publications by Year in descending order

Source: https://exaly.com/author-pdf/6327673/publications.pdf Version: 2024-02-01



#	Article	IF	CITATIONS
1	The fast azimuthal integration Python library: <i>pyFAI</i> . Journal of Applied Crystallography, 2015, 48, 510-519.	1.9	518
2	Thermal stability of retained austenite in TRIP steels studied by synchrotron X-ray diffraction during cooling. Acta Materialia, 2005, 53, 5439-5447.	3.8	460
3	Charge order and three-site distortions in the Verwey structure of magnetite. Nature, 2012, 481, 173-176.	13.7	424
4	Charge ordered structure of magnetiteFe3O4below the Verwey transition. Physical Review B, 2002, 66,	1.1	303
5	Long Range Charge Ordering in Magnetite Below the Verwey Transition. Physical Review Letters, 2001, 87, 266401.	2.9	295
6	Martensitic transformation of individual grains in low-alloyed TRIP steels. Scripta Materialia, 2007, 56, 421-424.	2.6	245
7	Characterization of individual retained austenite grains and their stability in low-alloyed TRIP steels. Acta Materialia, 2007, 55, 6713-6723.	3.8	226
8	Determining grain resolved stresses in polycrystalline materials using three-dimensional X-ray diffraction. Journal of Applied Crystallography, 2010, 43, 539-549.	1.9	175
9	High-energy X-ray diffraction study on the temperature-dependent mechanical stability of retained austenite in low-alloyed TRIP steels. Acta Materialia, 2012, 60, 565-577.	3.8	175
10	Grain-resolved analysis of localized deformation in nickel-titanium wire under tensile load. Science, 2016, 353, 559-562.	6.0	154
11	Rate-Induced Solubility and Suppression of the First-Order Phase Transition in Olivine LiFePO ₄ . Nano Letters, 2014, 14, 2279-2285.	4.5	148
12	X-ray transfocators: focusing devices based on compound refractive lenses. Journal of Synchrotron Radiation, 2011, 18, 125-133.	1.0	147
13	Direct view on the phase evolution in individual LiFePO4 nanoparticles during Li-ion battery cycling. Nature Communications, 2015, 6, 8333.	5.8	121
14	Quantifying Interparticle Forces and Heterogeneity in 3D Granular Materials. Physical Review Letters, 2016, 117, 098005.	2.9	109
15	PyFAI: a Python library for high performance azimuthal integration on GPU. Powder Diffraction, 2013, 28, S339-S350.	0.4	96
16	Multigrain crystallography. Zeitschrift Für Kristallographie, 2012, 227, 63-78.	1.1	95
17	Strong grain neighbour effects in polycrystals. Nature Communications, 2018, 9, 171.	5.8	92
18	The effect of aluminium and phosphorus on the stability of individual austenite grains in TRIP steels. Acta Materialia, 2009, 57, 533-543.	3.8	80

#	Article	IF	CITATIONS
19	FabIO: easy access to two-dimensional X-ray detector images in Python. Journal of Applied Crystallography, 2013, 46, 537-539.	1.9	75
20	In situ synchrotron study on the interplay between martensite formation, texture evolution and load partitioning in low-alloyed TRIP steels. Materials Science & Engineering A: Structural Materials: Properties, Microstructure and Processing, 2011, 528, 6407-6416.	2.6	68
21	Powder crystallography on macromolecules. Acta Crystallographica Section A: Foundations and Advances, 2008, 64, 169-180.	0.3	63
22	Study of 3-D stress development in parent and twin pairs of a hexagonal close-packed polycrystal: Part Il – crystal plasticity finite element modeling. Acta Materialia, 2015, 93, 235-245.	3.8	61
23	Grain-resolved elastic strains in deformed copper measured by three-dimensional X-ray diffraction. Materials Characterization, 2011, 62, 651-660.	1.9	60
24	Electronic orders in the Verwey structure of magnetite. Physical Review B, 2012, 85, .	1.1	59
25	Study of 3-D stress development in parent and twin pairs of a hexagonal close-packed polycrystal: Part I – in-situ three-dimensional synchrotron X-ray diffraction measurement. Acta Materialia, 2015, 93, 246-255.	3.8	56
26	High energy X-ray transfocator based on Al parabolic refractive lenses for focusing and collimation. Journal of Physics: Conference Series, 2009, 186, 012073.	0.3	51
27	Can intergranular force transmission be identified in sand?. Granular Matter, 2011, 13, 251-254.	1.1	51
28	Deformation-induced orientation spread in individual bulk grains of an interstitial-free steel. Acta Materialia, 2015, 85, 301-313.	3.8	50
29	Mechanical stability of individual austenite grains in TRIP steel studied by synchrotron X-ray diffraction during tensile loading. Materials Science & Engineering A: Structural Materials: Properties, Microstructure and Processing, 2014, 618, 280-287.	2.6	48
30	The Structure of Water in <i>p</i> â€Sulfonatocalix[4]arene. Chemistry - A European Journal, 2011, 17, 10259-10271.	1.7	46
31	Co-emergence of magnetic order and structural fluctuations in magnetite. Nature Communications, 2019, 10, 2857.	5.8	43
32	Resonant x-ray diffraction study of the charge ordering in magnetite. Journal of Physics Condensed Matter, 2005, 17, 7633-7642.	0.7	42
33	Second SH3 Domain of Ponsin Solved from Powder Diffraction. Journal of the American Chemical Society, 2007, 129, 11865-11871.	6.6	42
34	Solving Larger Molecular Crystal Structures from Powder Diffraction Data by Exploiting Anisotropic Thermal Expansion. Angewandte Chemie - International Edition, 2003, 42, 2029-2032.	7.2	40
35	Photostrictive/Piezomagnetic Core–Shell Particles Based on Prussian Blue Analogues: Evidence for Confinement Effects?. Journal of Physical Chemistry C, 2014, 118, 13186-13195.	1.5	40
36	Charge localization in the Verwey structure of magnetite. Physical Review B, 2015, 92, .	1.1	40

#	Article	IF	CITATIONS
37	Revealing metallic ink in Herculaneum papyri. Proceedings of the National Academy of Sciences of the United States of America, 2016, 113, 3751-3754.	3.3	40
38	Scanning 3DXRD Measurement of Grain Growth, Stress, and Formation of Cu6Sn5 around a Tin Whisker during Heat Treatment. Materials, 2019, 12, 446.	1.3	38
39	Reconstructing intragranular strain fields in polycrystalline materials from scanning 3DXRD data. Journal of Applied Crystallography, 2020, 53, 314-325.	1.9	36
40	Variable temperature powder neutron diffraction study of the Verwey transition in magnetite Fe3O4. Solid State Sciences, 2000, 2, 747-753.	1.5	34
41	Structural, magnetic, and spectroscopic studies of YAgSn, TmAgSn, and LuAgSn. Journal of Solid State Chemistry, 2006, 179, 2376-2385.	1.4	33
42	Friedel-pair based indexing method for characterization of single grains with hard X-rays. Materials Science & Engineering A: Structural Materials: Properties, Microstructure and Processing, 2009, 524, 64-68.	2.6	33
43	Grain interaction mechanisms leading to intragranular orientation spread in tensile deformed bulk grains of interstitial-free steel. International Journal of Plasticity, 2017, 88, 108-125.	4.1	32
44	High-throughput phase-diagram mappingviapowder diffraction: a case study of HEWLversuspH. Acta Crystallographica Section D: Biological Crystallography, 2005, 61, 1612-1625.	2.5	31
45	Spatiallyâ€Resolved Inâ€Situ Structural Study of Organic Electronic Devices with Nanoscale Resolution: The Plasmonic Photovoltaic Case Study. Advanced Materials, 2013, 25, 4760-4765.	11.1	31
46	On the nucleation of deformation twins at the early stages of plasticity. Acta Materialia, 2020, 196, 733-746.	3.8	31
47	Discovery and Structure Determination of an Unusual Sulfide Telluride through an Effective Combination of TEM and Synchrotron Microdiffraction. Angewandte Chemie - International Edition, 2015, 54, 10020-10023.	7.2	30
48	Extraction and use of correlated integrated intensities with powder diffraction data. Zeitschrift Fur Kristallographie - Crystalline Materials, 2004, 219, 791-802.	0.4	29
49	Impurity precipitation in atomized particles evidenced by nano x-ray diffraction computed tomography. Applied Physics Letters, 2014, 105, .	1.5	29
50	Heterogeneous grain-scale response in ferroic polycrystals under electric field. Scientific Reports, 2016, 6, 22820.	1.6	28
51	Operando and Postreaction Diffraction Imaging of the La–Sr/CaO Catalyst in the Oxidative Coupling of Methane Reaction. Journal of Physical Chemistry C, 2019, 123, 1751-1760.	1.5	28
52	Synchrotron X-ray powder diffraction study of hexagonal turkey egg-white lysozyme. Acta Crystallographica Section D: Biological Crystallography, 2005, 61, 423-432.	2.5	27
53	The Verwey structure of a natural magnetite. Chemical Communications, 2016, 52, 4864-4867.	2.2	25
54	New opportunities at the Materials Science Beamline at ESRF to exploit high energy nano-focus X-ray beams. Current Opinion in Solid State and Materials Science, 2020, 24, 100818.	5.6	25

#	Article	IF	CITATIONS
55	In situ synchrotron X-ray diffraction of ferroelastic La0.8Ca0.2CoO3 ceramics during uniaxial compression. Acta Materialia, 2006, 54, 2615-2624.	3.8	24
56	Nitridophosphateâ€Based Ultraâ€Narrowâ€Band Blueâ€Emitters: Luminescence Properties of <i>AE</i> P ₈ N ₁₄ :Eu ²⁺ (<i>AE</i> =Ca, Sr, Ba). Chemistry - A European Journal, 2020, 26, 7292-7298.	1.7	24
57	Polymorphism of microcrystalline urate oxidase fromAspergillus flavus. Acta Crystallographica Section D: Biological Crystallography, 2010, 66, 539-548.	2.5	23
58	In situ synchrotron analysis of lattice rotations in individual grains during stress-induced martensitic transformations in a polycrystalline CuAlBe shape memory alloy. Acta Materialia, 2011, 59, 3636-3645.	3.8	22
59	The thermodynamic effect of nonhydrostatic stress on the Verwey transition. Earth and Planetary Science Letters, 2012, 319-320, 207-217.	1.8	22
60	Structural studies of human insulin cocrystallized with phenol or resorcinol <i>via</i> powder diffraction. Acta Crystallographica Section D: Biological Crystallography, 2012, 68, 1632-1641.	2.5	22
61	On the calibration of high-energy X-ray diffraction setups. I. Assessing tilt and spatial distortion of the area detector. Journal of Applied Crystallography, 2014, 47, 1042-1053.	1.9	22
62	On the state of deformation in a polycrystalline material in three-dimension: Elastic strains, lattice rotations, and deformation mechanisms. International Journal of Plasticity, 2018, 106, 145-163.	4.1	22
63	Structure evolution of soft magnetic (Fe36Co36B19.2Si4.8Nb4)100â^'Cu (x= 0 and 0.5) bulk glassy alloys. Acta Materialia, 2015, 95, 335-342.	3.8	21
64	Multi-scale mechanics of granular solids from grain-resolved X-ray measurements. Proceedings of the Royal Society A: Mathematical, Physical and Engineering Sciences, 2017, 473, 20170491.	1.0	21
65	Structural modifications in sub-Tg annealed CuZr-based metallic glass. Materials Science & Engineering A: Structural Materials: Properties, Microstructure and Processing, 2017, 707, 245-252.	2.6	21
66	High-resolution powder X-ray data reveal the T ₆ hexameric form of bovine insulin. Acta Crystallographica Section D: Biological Crystallography, 2013, 69, 978-990.	2.5	20
67	Improving stability of organic devices: a time/space resolved structural monitoring approach applied to plasmonic photovoltaics. Solar Energy Materials and Solar Cells, 2017, 159, 617-624.	3.0	20
68	Human insulin polymorphism upon ligand binding and pH variation: the case of 4-ethylresorcinol. IUCrJ, 2015, 2, 534-544.	1.0	19
69	Direct Synthesis of Cubic ZrMo ₂ O ₈ Followed by Ultrafast In Situ Powder Diffraction. Journal of the American Chemical Society, 2009, 131, 17560-17562.	6.6	17
70	Comparison between a near-field and a far-field indexing approach for characterization of a polycrystalline sample volume containing more than 1500 grains. Journal of Applied Crystallography, 2014, 47, 1402-1416.	1.9	17
71	Three-dimensional experimental granular mechanics. Geotechnique Letters, 2015, 5, 236-242.	0.6	17
72	Novel crystalline phase and first-order phase transitions of human insulin complexed with two distinct phenol derivatives. Acta Crystallographica Section D: Biological Crystallography, 2015, 71, 819-828.	2.5	17

#	Article	IF	CITATIONS
73	Powder diffraction studies on proteins: An overview of data collection approaches. Zeitschrift Für Kristallographie, Supplement, 2007, 2007, 1-13.	0.5	16
74	High-Temperature Processing of Ba ₃ ZnTa ₂ O ₉ :  an In situ Study Using Synchrotron X-ray Powder Diffraction. Chemistry of Materials, 2007, 19, 4731-4740.	3.2	15
75	Cation ordering/disordering kinetics in Ba3CoNb2O9: An in situ study using synchrotron x-ray powder diffraction. Applied Physics Letters, 2007, 91, 222901.	1.5	15
76	Alignment of Plate-Like Particles in a Colloidal Dispersion under Flow in a Uniform Pipe Studied by High-Energy X-ray Diffraction. Langmuir, 2010, 26, 18701-18709.	1.6	15
77	Stability enhancement of organic photovoltaic devices utilizing partially reduced graphene oxide as the hole transport layer: nanoscale insight into structural/interfacial properties and aging effects. RSC Advances, 2015, 5, 106930-106940.	1.7	15
78	Quantitative grain-scale ferroic domain volume fractions and domain switching strains from three-dimensional X-ray diffraction data. Journal of Applied Crystallography, 2015, 48, 882-889.	1.9	15
79	Electromechanical Response of Polycrystalline Barium Titanate Resolved at the Grain Scale. Journal of the American Ceramic Society, 2017, 100, 393-402.	1.9	15
80	<i>Operando</i> Nanobeam Diffraction to Follow the Decomposition of Individual Li ₂ O ₂ Grains in a Nonaqueous Li–O ₂ Battery. Journal of Physical Chemistry Letters, 2016, 7, 3388-3394.	2.1	14
81	High-resolution powder neutron diffraction study of helimagnetic order inCrP1â^xVxO4solid solutions. Physical Review B, 2000, 62, 992-997.	1.1	13
82	In-situ observation of the nucleation kinetics and the mechanism of grain refinement in Al–Si alloys (Part I). Materials Letters, 2010, 64, 1016-1018.	1.3	13
83	Simultaneous X-ray diffraction from multiple single crystals of macromolecules. Acta Crystallographica Section D: Biological Crystallography, 2011, 67, 608-618.	2.5	13
84	Total scattering experiments on glass and crystalline materials at the ESRF on the ID11 Beamline. Powder Diffraction, 2015, 30, S2-S8.	0.4	13
85	Structure of lithium benzilate hemihydrate solved by simulated annealing and difference Fourier synthesis from powder data. Acta Crystallographica Section B: Structural Science, 2003, 59, 378-383.	1.8	12
86	Location of Mn sites in ferromagnetic Ga1â^'xMnxAs studied by means of X-ray diffuse scattering holography. Journal of Applied Crystallography, 2006, 39, 735-738.	1.9	12
87	Molecular envelopes derived from protein powder diffraction data. Journal of Applied Crystallography, 2008, 41, 329-339.	1.9	12
88	Advanced gas hydrate studies at ambient conditions using suspended droplets. Chemical Communications, 2011, 47, 9369.	2.2	12
89	Charge-density analysis using multipolar atom and spherical charge models: 2-methyl-1,3-cyclopentanedione, a compound displaying a resonance-assisted hydrogen bond. Acta Crystallographica Section B: Structural Science, Crystal Engineering and Materials, 2014, 70, 197-211.	0.5	12
90	Cationic Pb ₂ Dumbbells Stabilized in the Highly Covalent Lead Nitridosilicate Pb ₂ Si ₅ N ₈ . Angewandte Chemie - International Edition, 2019, 58, 1432-1436.	7.2	12

#	Article	IF	CITATIONS
91	Formation and annihilation of stressed deformation twins in magnesium. Communications Materials, 2021, 2, .	2.9	12
92	Successful protein cryocooling for powder diffraction. Journal of Applied Crystallography, 2007, 40, 121-124.	1.9	11
93	Domain switching in rhombohedral PZT ceramics under electrical and mechanical loading. Materials Science and Technology, 2008, 24, 927-933.	0.8	11
94	Time-dependent analysis of K2PtBr6binding to lysozyme studied by protein powder and single crystal X-ray analysis. Zeitschrift Für Kristallographie, 2010, 225, 570-575.	1.1	11
95	Dense SixGe1–x (0 < x < 1) Materials Landscape Using Extreme Conditions and Precession Electron Diffraction. Inorganic Chemistry, 2014, 53, 5656-5662.	1.9	11
96	Coxsackievirus B3 protease 3C: expression, purification, crystallization and preliminary structural insights. Acta Crystallographica Section F, Structural Biology Communications, 2016, 72, 877-884.	0.4	11
97	Exploiting Confinement to Study the Crystallization Pathway of Calcium Sulfate. Advanced Functional Materials, 2021, 31, 2107312.	7.8	11
98	Deciphering mineralogical changes and carbonation development during hydration and ageing of a consolidated ternary blended cement paste. IUCrJ, 2018, 5, 150-157.	1.0	11
99	Nitridic Analogs of Micas <i>AE</i> Si ₃ P ₄ N ₁₀ (NH) ₂ (<i>AE</i> =Mg, Mg _{0.94} Ca _{0.06} , Ca, Sr). Angewandte Chemie - International Edition, 2022, 61, e202114902.	7.2	11
100	Features of the secondary structure of a protein molecule from powder diffraction data. Acta Crystallographica Section D: Biological Crystallography, 2010, 66, 756-761.	2.5	10
101	Planar Perovskite Solar Cells: Local Structure and Stability Issues. Solar Rrl, 2017, 1, 1700066.	3.1	10
102	Quantifying local rearrangements in three-dimensional granular materials: Rearrangement measures, correlations, and relationship to stresses. Physical Review E, 2022, 105, 014904.	0.8	10
103	Intermetallic phase detection in lead-free solders using synchrotron x-ray diffraction. Journal of Electronic Materials, 2004, 33, 1524-1529.	1.0	9
104	Residual stress relief due to fatigue in tetragonal lead zirconate titanate ceramics. Journal of Applied Physics, 2013, 114, 024103.	1.1	9
105	Information on real-structure phenomena in metastable GeTe-rich germanium antimony tellurides (GeTe)nSb2Te3 (n ≥ 3) by semi-quantitative analysis of diffuse X-ray scattering. Zeitschrift Fur Kristallographie - Crystalline Materials, 2015, 230, .	0.4	9
106	The Crystal Structure of Ba3Cu2Al2F16: a Relative of Ba4Cu2Al3F21. Zeitschrift Fur Anorganische Und Allgemeine Chemie, 2003, 629, 1960-1964.	0.6	8
107	Preliminary insights into the non structural protein 3 macro domain of the Mayaro virus by powder diffraction. Zeitschrift Für Kristallographie, 2010, 225, .	1.1	8
108	Progressive melting in confined one-dimensional C <mml:math xmlns:mml="http://www.w3.org/1998/Math/MathML" display="inline"><mml:msub><mml:mrow /><mml:mn>60</mml:mn></mml:mrow </mml:msub>chains. Physical Review B, 2012, 86, .</mml:math 	1.1	8

#	Article	IF	CITATIONS
109	Optimizing shape uniformity and increasing structure heights of deep reactive ion etched silicon x-ray lenses. Journal of Micromechanics and Microengineering, 2015, 25, 125013.	1.5	8
110	Dithiophene-TTF Salts; New Ladder Structures and Spin-Ladder Behavior. Inorganic Chemistry, 2015, 54, 7000-7006.	1.9	8
111	RE4Ba2[Si12O2N16C3]:Eu2+ (RE = Lu, Y): Green-Yellow Emitting Oxonitridocarbidosilicates with a Highly Condensed Network Structure Unraveled through Synchrotron Microdiffraction. Inorganic Chemistry, 2018, 57, 13840-13846.	1.9	8
112	Site-selective doping of ordered charge states in magnetite. Nature Communications, 2020, 11, 1671.	5.8	8
113	Exploiting X-ray induced anisotropic lattice changes to improve intensity extraction in protein powder diffraction: Application to heavy atom detection. Zeitschrift Für Kristallographie, Supplement, 2007, 2007, 39-44.	0.5	8
114	Partial frustration of magnetic order in synthetic angelellite, Fe4As2O11 â€. Dalton Transactions RSC, 2000, , 3663-3668.	2.3	7
115	Experimental verification of dynamical diffraction focusing by a bent crystal wedge in Laue geometry. Journal of Applied Crystallography, 2008, 41, 695-700.	1.9	7
116	The verwey phase of magnetite — a long-running mystery in magnetism. Journal of the Korean Physical Society, 2013, 62, 1372-1375.	0.3	7
117	Pressure-induced structural and magnetic phase transitions in ordered and disordered equiatomic FeCo. Physical Review B, 2013, 88, .	1.1	7
118	Creating Reactivity with Unstable Endmembers using Pressure and Temperature: Synthesis of Bulk Cubic Mg _{0.4} Fe _{0.6} N. Angewandte Chemie - International Edition, 2015, 54, 15109-15112.	7.2	7
119	Revealing Operando Transformation Dynamics in Individual Li-ion Electrode Crystallites Using X-Ray Microbeam Diffraction. Frontiers in Energy Research, 2018, 6, .	1.2	7
120	BaP ₆ N ₁₀ NH:Eu ²⁺ as a Case Study–An Imidonitridophosphate Showing Luminescence. Chemistry - A European Journal, 2020, 26, 5010-5016.	1.7	7
121	Crystal structure determination of a lifelong biopersistent asbestos fibre using single-crystal synchrotron X-ray micro-diffraction. IUCrJ, 2021, 8, 76-86.	1.0	7
122	Beam heating from a fourth-generation synchrotron source. Journal of Synchrotron Radiation, 2021, 28, 1377-1385.	1.0	7
123	Depicting the crystal structure of fibrous ferrierite from British Columbia using a combined synchrotron techniques approach. Journal of Applied Crystallography, 2019, 52, 1397-1408.	1.9	7
124	Effect of iron on delithiation in LixCo1â^'yFeyO2. Part 1: in-situ electrochemical and X-ray diffraction study. Journal of Materials Chemistry, 2004, 14, 94-101.	6.7	6
125	The texture of Nd oxide grains in Nd-Fe-B sintered magnets studied by synchrotron radiation. Journal of Applied Physics, 2011, 110, 026103.	1.1	6
126	Synthesis and high-resolution study distinguishing between very similar interstitial iron nitride structures. High Pressure Research, 2015, 35, 28-36.	0.4	6

#	Article	IF	CITATIONS
127	Likelihood methods with protein powder diffraction data. Zeitschrift Für Kristallographie, Supplement, 2007, 2007, 27-32.	0.5	6
128	Synchrotron Nano-Diffraction Study of Thermally Treated Asbestos Tremolite from Val d'Ala, Turin (Italy). Minerals (Basel, Switzerland), 2018, 8, 311.	0.8	5
129	Using Powder Diffraction Patterns to Calibrate the Module Geometry of a Pixel Detector. Crystals, 2022, 12, 255.	1.0	5
130	Helimagnetic order in ferric arsenate, FeAsO4. Journal of Physics Condensed Matter, 1999, 11, 1473-1478.	0.7	4
131	The low-temperature structure of nopinone. Zeitschrift Für Kristallographie, 2008, 223, 602-604.	1.1	4
132	Solid solution along the synthetic LiAlSi ₂ O ₆ -LiFeSi ₂ O ₆ (spodumene-ferri-spodumene) join: A general picture of solid solutions, bond lengths, lattice strains, steric effects, symmetries, and chemical compositions of Li clinopyroxenes. American Mineralogist, 2016, 101, 2498-2513.	0.9	4
133	Probing structural chirality with high-energy synchrotron radiation. Journal of Applied Crystallography, 2016, 49, 918-922.	1.9	4
134	Electronic origin of negative thermal expansion in V2OPO4. Chemical Communications, 2020, 56, 6523-6526.	2.2	4
135	X-ray Diffraction Computed Nanotomography Applied to Solve the Structure of Hierarchically Phase-Separated Metallic Glass. ACS Nano, 2021, 15, 2386-2398.	7.3	4
136	Nitridic Analogs of Micas AESi3P4N10(NH)2 (AE = Mg, Mg0.94Ca0.06, Ca, Sr). Angewandte Chemie, 2022, 134, e202114902.	1.6	4
137	Multi-scale in situ mechanical investigation of the superelastic behavior of a Cu–Al–Be polycrystalline shape memory alloy. Acta Materialia, 2022, 235, 118107.	3.8	4
138	Crystallographic Phase Composition and Structural Analysis of Ti-Ni-Fe Shape Memory Alloy by Synchrotron Diffraction. Solid State Phenomena, 2005, 105, 139-144.	0.3	3
139	Residual and bending stress measurements by X-ray diffraction and synchrotron diffraction analysis in silicon solar cells. , 2012, , .		3
140	Multi length scale characterization of austenite in TRIP steels using high-energy X-ray diffraction. Powder Diffraction, 2013, 28, 77-80.	0.4	3
141	High-resolution X-ray diffraction investigation on the evolution of the substructure of individual austenite grains in TRIP steels during tensile deformation. Journal of Applied Crystallography, 2014, 47, 965-973.	1.9	3
142	High temperature investigation of SiO2-Al2O3-ZnO-Na2O glass for ceramic-glaze: inâ€situ/ex-situ synchrotron diffraction and conventional approaches. Ceramics International, 2018, 44, 6395-6401.	2.3	3
143	X-ray diffraction and heterogeneous materials: An adaptive crystallography approach. Comptes Rendus Physique, 2018, 19, 553-560.	0.3	3
144	In situ synchrotron analysis of phase transformation at high temperatures in ODS ferritic steel. Journal of Materials Science, 2020, 55, 5600-5612.	1.7	3

#	Article	IF	CITATIONS
145	Texture Memory in Si-Mn and ODS Steels Observed In Situ by Pulsed Neutron and Synchrotron X-Ray Diffractions and Prediction by Double Kurdjumov-Sachs Relation: A Concept for Intense Variant Selection. Metallurgical and Materials Transactions A: Physical Metallurgy and Materials Science, 2021, 52, 1368-1381.	1.1	3
146	Hexagonal Siâ^'Ge Class of Semiconducting Alloys Prepared by Using Pressure and Temperature. Chemistry - A European Journal, 2021, 27, 14217-14224.	1.7	3
147	Non-destructive determination of phase, size, and strain of individual grains in polycrystalline photovoltaic materials. Journal of Alloys and Compounds, 2021, 887, 161364.	2.8	3
148	Design and Technical Aspects of a New in Vacuum Transfocator at ESRF Beamline ID11. , 2010, , .		2
149	Measurement of lattice rotations and internal stresses in over one hundred individual grains during a stress-induced martensitic transformation. MATEC Web of Conferences, 2015, 33, 02003.	0.1	2
150	Force measurements in stiff, 3D, opaque granular materials. EPJ Web of Conferences, 2017, 140, 02006.	0.1	2
151	Effects of resolution in real and reciprocal spaces from a 2D detector at a high-energy synchrotron beamline. Powder Diffraction, 2018, 33, 11-20.	0.4	2
152	Micromechanics of Granular Media Characterised Using X-Ray Tomography and 3DXRD. Trends in Mathematics, 2018, , 169-176.	0.1	2
153	Serial crystallography for the masses?. IUCrJ, 2015, 2, 3-4.	1.0	2
154	Powder Diffraction Refinements of the Structure of Magnetite (Fe3O4) Below the Verwey Transition. Materials Research Society Symposia Proceedings, 2000, 658, 261.	0.1	1
155	Structures of (S)-(â^')-4-oxo-2-azetidinecarboxylic acid and 3-azetidinecarboxylic acid from powder synchrotron diffraction data. Acta Crystallographica Section B: Structural Science, 2006, 62, 606-611.	1.8	1
156	lmaging of interstitial atoms in Ga _{1â^'<i>x</i>} Mn _{<i>x</i>} As layers by means of X-ray diffuse scattering. Journal of Applied Crystallography, 2008, 41, 544-547.	1.9	1
157	Local elasticity and macroscopic plasticity in homogeneous and heterogeneous bulk metallic glasses. Applied Physics Letters, 2019, 115, 141901.	1.5	1
158	An Application of Multigrain Approaches to the Structural Solution of Grains from Polycrystalline Samples. Solid State Phenomena, 2019, 288, 119-123.	0.3	1
159	Successful cryocooling of protein microcrystalline samples for powder diffraction. Acta Crystallographica Section A: Foundations and Advances, 2009, 65, s320-s321.	0.3	1
160	High-Energy Synchrotron Radiation Research at the ESRF. Synchrotron Radiation News, 2020, 33, 5-10.	0.2	1
161	The Crystal Structure of Ba3Cu2Al2F16: A Relative of Ba4Cu2Al3F21 ChemInform, 2004, 35, no.	0.1	0
162	Time-resolved binding of K2PtBr6to lysozyme by protein powder and single-crystal X-ray. Acta Crystallographica Section A: Foundations and Advances, 2009, 65, s80-s81.	0.3	0

#	Article	IF	CITATIONS
163	Ordering phenomena in minerals: the Verwey phase of natural magnetite. Acta Crystallographica Section A: Foundations and Advances, 2017, 73, C1302-C1302.	0.0	0
164	Extracting structural information from protein powder diffraction data. Acta Crystallographica Section A: Foundations and Advances, 2006, 62, s232-s232.	0.3	0
165	Molecular envelopes from protein powder diffraction data. Acta Crystallographica Section A: Foundations and Advances, 2007, 63, s76-s76.	0.3	0
166	High-throughput phase diagram mapping of urate oxidaseviapowder diffraction. Acta Crystallographica Section A: Foundations and Advances, 2009, 65, s321-s322.	0.3	0
167	Proteins and Powders: Technical Developments. NATO Science for Peace and Security Series B: Physics and Biophysics, 2012, , 125-135.	0.2	0
168	Ordering phenomena in minerals: the Verwey phase of natural magnetite. Acta Crystallographica Section A: Foundations and Advances, 2016, 72, s63-s63.	0.0	0
169	Water-rock interactions in carbonaceous chondrites: a meso to nanoscale study of alteration processes in an anoxygenic environment. Acta Crystallographica Section A: Foundations and Advances, 2016, 72, s70-s70.	0.0	0
170	Likelihood methods with protein powder diffraction data. Zeitschrift Für Kristallographie, 2007, 2007, 27-32.	1.1	0
171	Exploiting X-ray induced anisotropic lattice changes to improve intensity extraction in protein powder diffraction: Application to heavy atom detection. Zeitschrift Für Kristallographie, 2007, 2007, 39-44.	1.1	0